New investigation on global efficiency in thermal power plants, addressing the environmental impact of burning alternative fuels through CFD

Jesús M. Blanco, Lakhdar Remaki and Francisco Peña

***Abstract*—** Traditional fossil fuels stocks are limited so are considered "non-renewable" whereas bio-fuels are "renewable" sources. Nowadays, the possibility of converting fuel oil into natural gas fired power plants has risen due to a global concern about the "greenhouse effect". On the one hand, the main advantages are that the acidic emissions are almost annulled while monetary incentives were introduced into particular statutory regulation schemes. On the other hand, disadvantages are mainly the high traces of ashes that gas matrix contains, causing the exhaust gases strong abrasive scratches over hot surfaces. A particular gas derived from biomass obtained in fluidized beds has been revealed as a credible option. First of all, a full theoretical evaluation of the global efficiency associated to a power plant of reference depending on the fuel burned has been performed and improved significantly with the proper determination of the so called "difficult evaluation losses term", demonstrating the suitability of fuel replacement in terms of efficiency. The main contribution corresponds to a CFD study, validated through the results provided by a scaled experimental facility, fully monitored, in order to compare the environmental impact of two of these fuels, justifying its use for further characterizations of other fuels prior to its full implementation.

***Keywords*—** Alternative fuels, bio gas, CFD, efficiency, natural gas.

I. Introduction

Fossil fuels stocks are limited and are considered non-renewable sources. From the decade of the 90´s, the possibility of converting fuel oil (FO) fired power plant into natural gas (NG) has been raised [1, 2], due mainly to the significant increasing in the global concern about the "greenhouse effect".

Natural gas expectations as fuel replacement in some sectors are suffering a substantial increase but the most important fact is that recent increases in crude oil prices have brought alternative fuels into the energy scenario. Figure 1 shows the Gross Consumption of Natural Gas by the Organization for Economic Co-operation and Development (OECD). Source monthly gas survey 2015 IEA Statistics.

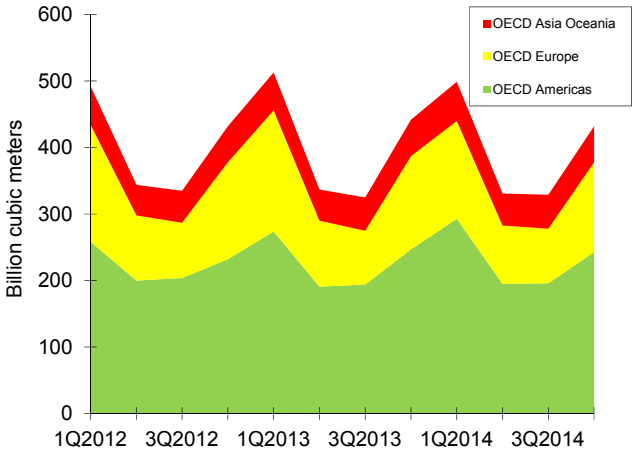

Fig. 1 Gross Consumption of Natural Gas by OECD Region.

General Electric, Pratt & Whitney, and other gas turbine manufacturers, have been testing these fuels in their machines for a long time [3, 4]. Today, bio-fuels have an additional attraction as they are considered "renewable sources" which is a strong argument for the success of their implementation [5, 6]. Note that special attention has to be paid to technical and operational challenges have to be taken into account regarding any fuel replacement issues [7].

Gas derived from biomass (BG) obtained in fluidized beds has been revealed as a credible option. There is an important source of biomass called "Miscanthus giganteus" for the production of energy either for direct combustion or through cellulosic ethanol as has been treated here. The gas matrix contains high traces of ashes [8], which are crucial to be eliminated, otherwise the gas would not be suitable for burning in gas turbines due to the enormous abrasive action of the exhaust gases caused by the high temperature (around 800ºC) combined with a high speed around the blades as

This work was supported in part by the University of the Basque Country under special project OPCOFLUID 2012-2015.

J. M. Blanco is with the Department of Nuclear Engineering and Fluid Mechanics, School of Engineering, University of the Basque Country, Bilbao, SPAIN (corresponding author phone: +34946014250; fax: +34946014043; e-mail: jesusmaria.blanco@ehu.es).

L. Remaki, is with BCAM, Basque Center for Applied Mathematics, Bilbao, SPAIN (e-mail: lremaki@bcamath.org).

F. Peña is collaborating with the Department of Nuclear Engineering and Fluid Mechanics, School of engineering, University of the Basque Country, Bilbao, SPAIN (e-mail: fpfbg@telefonica.net).

described in [9].

Key driving factors for bio-fuels are the monetary incentives built into particular regulations of each estate which makes it difficult to evaluate and compare among different countries [10]. Too many questions arise in order to make a clear decision at least in the near future as these alternative fuels are still not available in sufficient volume all over the world for supporting the current power generation [11].

There is also another significant challenge as conventional power plants have been gradually replaced by combined cycles around the world. The most commonly fuel burned in conventional cycles has been the fuel oil (FO); the so called "$N^{er}2$" and the low sulphur index fuel (LSI) have been traditionally used in the main thermal power plants in Spain. Their substitution for NG has been widely proposed because its basic component methane (CH_4), contributes to the greenhouse effect by about 18 % while SO_2 emissions are almost annulled [12 - 14]. First of all, the advantages of burning some of these fuels have been demonstrated through this paper in terms of efficiency, with data from a power plant of reference.

Finally a complete CFD (Computational Fluid Dynamics) model was built and validated later on through the measurements obtained from an experimental facility designed and built ready for burning different fuels instead of burning them directly in the fossil-fuelled thermal power plant. Two different fuels were tested in this paper such as natural gas and a gas derived from biomass, in order to compare emissions.

II. Aims and Methodology

The aim of the present work is to show the overall effect of the gradual replacement of fossil fuel consumption for natural gas, or other alternative fuels such as bio-fuels, in terms of efficiency and emissions, ensuring combustion quality.

It is crucial to point out that the global efficiency in a thermal power plant on the base of the LCV is around 39 % in case of conventional cycles [15], so the assessment of this particular situation when burning different fuels is another relevant objective. First of all, the boiler and global efficiencies for conventional cycles burning fossil and alternative fuels will be determined based on both gross and lower calorific values on a thermal power plant of reference.

Finally, the advantages of burning some of these fuels will be demonstrated through a CFD (Computational Fluid Dynamics) model, validated by the measurements obtained through an experimental scaled combustion chamber, which will be fully described later, ready for burning different fuels, so a comparative test between NG and BG will be performed.

III. Determination of the Global Efficiency

A. Procedure

The global efficiency of a power plant can be calculated according to Eq. 1,

$$\eta_G = \eta_c \times \eta_b \tag{1}$$

Whereas the cycle efficiency reaches a constant value of 0.41 regardless of the fuel type burned, the global efficiency can be directly obtained through the boiler efficiency which can be associated to the low or gross calorific values of the fuel burned [16] according to Eqs. 2 and 3, respectively.

$$\eta_{b(GCV)} = \frac{\left(GCV + \sum fCr\right) - \sum_{GCV} P}{GCV + \sum fC_r} \tag{2}$$

$$\eta_{b(LCV)} = \frac{\left(LCV + \sum fCr\right) - \left(\sum_{GCV} P - Q_{lat(vap)}\right)}{LCV + \sum fCr} \tag{3}$$

Where:

$$Q_{lat(vap)} = r \times m_{vap} \tag{4}$$

Considering for the water (at 20ºC) according to *ASTM D 240-50*,

$$r = 2{,}436.31\ {}^{kJ}\!/_{kg} \tag{5}$$

Relationship between LCV and GCV is given by:

$$LCV = GCV \cdot (1 - H) - r \cdot (A + H) \tag{6}$$

On the one hand, the total losses term can be split into several terms, according to,

$$\sum_{GCV} P = P_{dg} + P_{wf} + P_{H2} + P_{wa} + P_{CO} + P_{de} + P_{CR} \tag{7}$$

Where the different terms can be defined as:

$$P_{dg} = \dot{m}_{dg} \times Cp_{dg} \times \left(T_{dg} - T_{ext}\right) \tag{8}$$

$$P_{wf} = 0 \tag{9}$$

$$P_{H2} = m_{H2} \times \left(h_{vap} - h_{ext}\right) \tag{10}$$

$$P_{wa} = x \times m_{da} \times \left(h_{vap} - h_{sat}\right) \tag{11}$$

$$P_{CO} = \frac{[CO]_v}{[CO_2 + CO]_v} \times 5.632 \times [CO]_m \tag{12}$$

$$P_{de} = \left(\frac{DE}{100}\right) \times GCV \tag{13}$$

$$P_{CR} = P_C + P_R \tag{14}$$

Splitting this term into convection and radiation losses:

$$P_C = \frac{Q_C \times S_{bw}}{m_f} \tag{15}$$

$$P_R = \frac{Q_R \times S_{bw}}{\dot{m}_f} \tag{16}$$

$$Q_C = 2.712 \times \left(1 + 0.0225 \cdot v\right) \times \left(T_{bw} - T_{ext}\right) \tag{17}$$

$$Q_R = 47.188 \times 10^{-10} \times \varepsilon \times \left(T_{bw}^4 - T_{ext}^4\right) \tag{18}$$

Where the total surface boiler of the thermal power plant of reference was divided into N areas according to their respective temperatures, being

$$S_{bw} = \sum_{i=1}^{N} S_{bwi} \tag{19}$$

The calculation of the average temperature for the boiler walls can be obtained according to the average temperature (T_{bwi}) assigned to each one of these areas:

$$T_{bw} = \frac{\sum_{i=1}^{N} T_{bwi} \times S_{bwi}}{S_{bw}} \tag{20}$$

For the dry gases,

$$C_{p_{dg}} = a + b \cdot T_{dg} + c \cdot T_{dg}^2 + d \cdot T_{dg}^3 \tag{21}$$

Whose constants are shown next in Table 1,

Table 1. Definition of Cp constants for the dry gases

(kJ kg^{-1} K^{-1})	**a**	**b × 10^2**	**c × 10^5**	**d × 10^9**
N_2	6.903	– 0.03753	0.1930	0.6861
O_2	6.085	0.3631	– 0.1709	0.3133
CO_2	5.316	1.4285	– 0.8362	1.784

Special treatment will be given to the so called "Difficult evaluation losses term" (P_{de}). This is in fact the sum of a set of minor entity losses such as, ashes radiation heat, sensitive heat of slags, latent heat of fusion of slags, unburned hydrocarbons, and formation of free radicals and species dissociation respectively.

Due to their special nature, the direct and rigorous evaluation of the three first terms turns to be really complex whereas the evaluation of the last two ones is simply impossible, given that the combustion is reached inside great boilers with burners in turbulent flow regime.

On the other hand, the credit factors are given by:

$$\sum fCr = fCr_a + fCr_p \tag{22}$$

Where the two different terms on the right side of this equation, associated to air comburent and boiler recirculation water pumps respectively can be defined as:

$$fCr_a = Cp_a \times \dot{m}_a \times \left(T_{heat} - T_{ext}\right) \tag{23}$$

$$fCr_p = 0.5 \times \frac{Ep}{\dot{m}_f} \tag{24}$$

The later equation considers than only half of the full load electrical consumption of the pumps *Ep* is transferred. This approximations is usually accepted when burning these fuels [13].

B. Application to a case study

The next considerations must be taken into account for this particular approach:

- Averaged temperature for dry gases is (T_{dg} = 85 ºC).
- The percentage of carbon that gets transformed to CO, admitting a good operative practice of the boiler together with a suitable design of this one, provides values between 4 and 20 mg Nm^{-3}.
- The specific losses associated with convection and radiation (kJ $^{h-1}$ $^{m-2}$) respectively was proposed by ASTM Committee C-8, Subcommittee on heat transfer, 1937 (revised on 1947). A constant value of for the averaged air velocity (v = 1.5 m $^{s-1}$) is considered.
- The total boiler wall area (S_{bw} = 3,370 m^2) has been divided into N = 56 walls according to their temperature.
- The boiler walls temperature is assumed to be a constant value (T_{bw} = 54 ºC), being T_{ext} = 22 ºC.
- For the evaluation of these losses, a value of DE = 1 % (kJ per kilogram of fuel burned over the GCV) is commonly applied. Here nevertheless a value of DE = 1.078 % will be applied with the exception of DE = 1.92 % for the biomass derived fuel [13].
- The temperature of the air prior to the preheater (Ljungstron type) is assumed to be a constant value (T_{heat} = 46 ºC) whereas (Cp_a = 1 kJ kg^{-1} K^{-1}).
- A full load electrical consumption of the pumps: (E_p = 985 kWh) has been considered.
- The credit factor associated to the boiler recirculation pumps (kJ per kilogram of fuel burned) considers that only 50% of the energy supplied by the boiler pumps is transferred to heat the water inside the boiler.
- The averaged composition of the fuels addressed in this study can be seen in Tables 2 and 3 respectively.

Table 2. Volumetric composition of the Natural gas

(% vol.)	**Max.**	**Min.**	**Avgd.**
CH_4	89.8872	88.8317	88.9786
C_2H_6	5.1343	5.8767	5.1274
C_3H_8	1.2888	1.2662	1.2714
I-butane	0.2354	0.2249	0.2262
N-butane	0.3338	0.3283	0.3311
I-pentane	0.0794	0.0713	0.0727
N-pentane	0.0749	0.0718	0.0724
C_6H_{14}	0.1223	0.1177	0.1200
N_2	3.5393	3.4742	3.4898
CO_2	0.4185	0.2996	0.3112

Table 3. Mass composition for the rest of fuels

(% mass)	**FO "N 2"**	**FO "LSI"**	**BG**
C	85.40	85.98	43.13
H2	10.38	10.91	6.31
N2	0.55	0.46	0.46
O2	0.00	1.54	47.28
S	2.92	0.81	0.00
Moisture	0.45	0.00	0.00
Ash	0.30	0.30	2.82

- Finally, Table 4 shows the main technical details of the thermal power plant of reference.

Table 4. Technical details of the thermal power plant

Net power (MW)	377
Minimum technical load (MW)	140
Fuel consumption (ton/day)	2,900
Boilers (Babcock & Wilcox)	
• **Vapour production (ton/h)**	1,735
• **Reheater out temp. (ºC)**	540.5
• **Reheater out press (kg/cm^2)**	42.67
Turbine/alternator (G E)	
• **Inlet temperature (ºC)**	538
• **Inlet pressure (kg/cm^2)**	40
• **Speed (rpm)**	3,000
• **Voltage (V)**	20,000
• **Electrical power (kVA)**	640,000 (cosφ = 0.85)
Air preheaters (American St.)	
• **Type**	H2M-23-120
• **Fluid**	Vapour
Fans (American St.)	
• **Type**	Double inlet
• **Number**	2
• **Motor power (kW) per unit**	1,840
Condensator (B&W)	
• **Number of steps/shell**	2
• **Type**	Surface
Water pumps (Ingersoll Rand)	
• **Number**	2
• **Motor power (kW) per unit**	2,826
Condensated pumps (Worth.)	
• **Number**	2
• **Motor power (kW) per unit**	766

C. Results

A breakdown of the different losses and credit factors previously defined are shown in Table 5 for all the fuels. Note the LCV for all the fuels are defined in the first row.

Table 5. Losses and credit factors for the different fuels

(kJ kg^{-1})	FO "N 2"	FO "LSI"	NG	BG
LCV	40,035.66	40,630.68	46,541.91	15,598.54
$\mathbf{P_{dg}}$	1,937.64	1,937.64	2,163.65	811.63
$\mathbf{P_{wf}}$	12.12	0.00	0.00	0.00
$\mathbf{P_{H2}}$	2,498.09	2,498.09	5,858.56	1,518.84
$\mathbf{P_{wa}}$	30.76	30.76	36.11	2.96
$\mathbf{P_{CO}}$	1.08	1.08	1.08	0.58
$\mathbf{P_{CR}}$	61.44	61.44	61.44	24.53
$\mathbf{P_{de}}$	1,393.69	1,145.44	556.82	325.87
$\mathbf{fCr_a}$	383.51	383.51	380.04	151.52
$\mathbf{fCr_p}$	20.56	20.56	20.56	8.19

So, the boiler efficiency can be calculated according to Eqs. 2 and 3, while the global efficiency can be determined according to Eq. 1. Figure 2 summarizes this for all the fuels considered here.

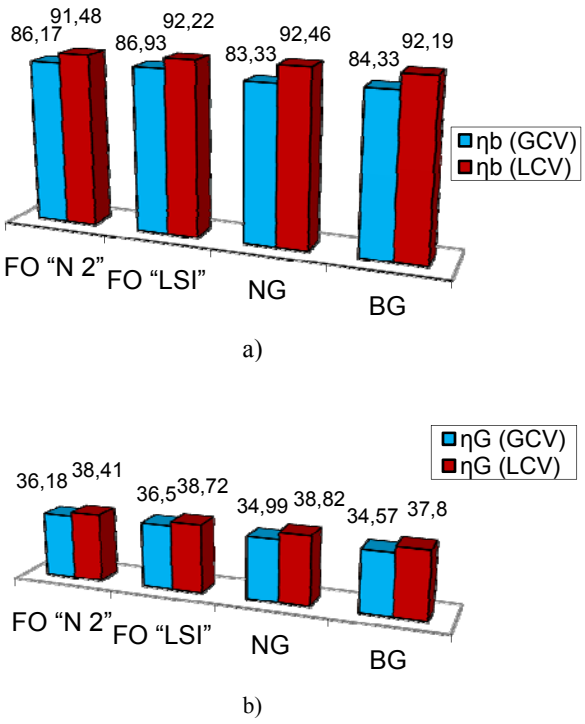

Fig. 2 Comparative test of efficiency, a) boiler; b) global

The most important conclusion is that boiler and global efficiencies present comparable values for all the fuels so alternative fuels could be considered an efficient option in thermal power plants regarding efficiency.

IV. Experimental Work

Experimental results have been achieved through direct measurements over a 465 kW thermal power experimental installation which is basically composed of a 4 m length combustion chamber whose walls are fully protected with glass fibre of 70 mm. thickness and equipped with a control board composed by two thermostats, a clock of temperature and pressure and a safety thermostat. Figure 3, shows a picture of the burner and redefined combustion chamber placed in our premises.

The chamber consists of three parts: fuel supply unit, adapted burner, and finally the boiler. The air is supplied by a centrifugal fan and passes outside through 12 uniformly-placed nozzles, where the fuel is finally injected, producing the required air-fuel mixture while the initiating spark produces the flame.

Figure 4 shows the basic scheme of the BG supply system. After this treatment, the bio-gas is ready to be fired in the combustion chamber.

The measurement process was considered as a decisive part of the design process and hence carefully designed. Four reference parts were carefully studied inside the chamber such as, chimney, combustion chamber, water and fuel respectively, so the numerical model will be fully adapted to them as it will play a decisive part in the validation procedure carried out, which will be described later.

Fig. 3 Picture of the fully monitored facility

For each one of these parts, several physical quantities were measured in order to guarantee that the information further needed for the *CFD* model would be precise enough. A 20 channels data-logger with complex software was used. The instrumentation used is briefly described below:

- *Temperature*: Ambient temperature is mostly measured using a platinum thermostat while flue gas temperature was measured at several points by a thermocouple. The following equipments were used for the measurement of the maximum temperature of the flame and of the walls of the combustion chamber: a wet-bulb thermometer, a resistance thermometer, thermocouples, and a portable colorimetric pyrometer, model QL2500.
- *Pressure*: Bourdon gauge of graduated mask, pressure differential cut-out and differential gauges.
- *Barometric pressure*: Standard aneroid barometer.
- *Flow*: Perforated plate (certified), for measuring the water flow, a differential gauge of 4-20 mA. (exit), for measuring the pressure drop, and a digital flow meter, model RMC205 for measuring the gas flow.
- Emissions: RS232C is a microprocessor-based gas analyser with a totally automatic microprocessor-based operation including auto start-up, auto-calibration, auto-range, internal parameter monitoring and alarms. Figure 5 shows the large multifunction 5" LCD monitor, providing a clear display values for different emissions and ambient temperatures as shown in Table 6.

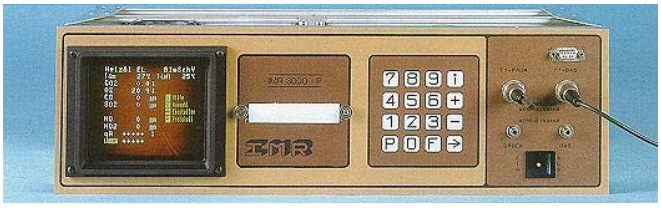

Fig. 5 Front view of the portable IMR3000 gas analyzer

Table 6. Main specifications of the gas analyzer

Response Time	5 s
Accuracy	+/- 1.0 %
Linearity	0.5 %
Max. Temp.	1,500 °C
Battery	12 VDC (6h autonomy)
Interface	RS 232 C
Memory	10,485 measurements
Units	ppm, mg/Nm^3
Emissions	CO, CO_2, SO_2, O_2, NO, NO_2, H_2S
Dimensions	510 x 180 x 430 mm
Weight	Aprox. 16 kg

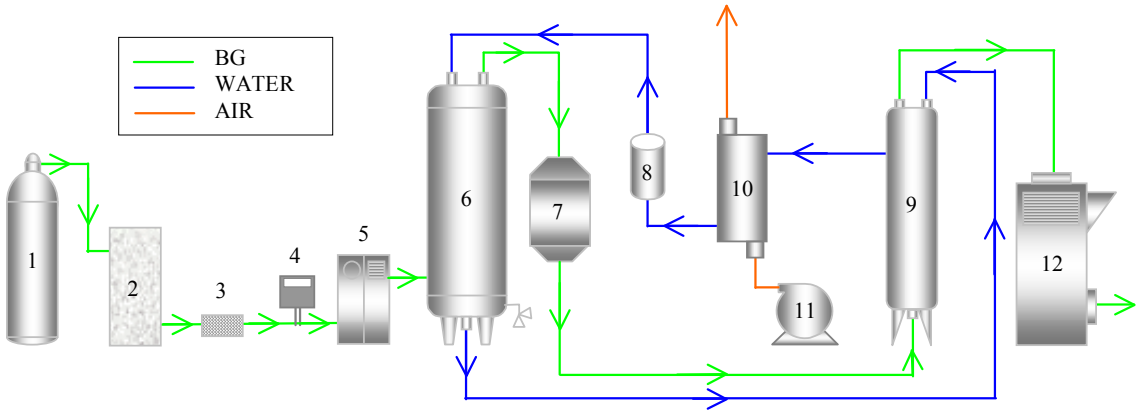

1. Bio-gas bottle.
2. Fractionation column.
3. Filter.
4. Gas analyzer.
5. M. C. S.
6. Odorization device.
7. Desulphurization unit.
8. Particle filter.
9. Water scrubbing column.
10. Heat exchanger.
11. Fan.
12. Through-drying machine.

Fig. 4. Basic scheme of the BG supply unit.

These outcomes provide enough information to define properly the boundary conditions and the validation of the CFD model that will be described next.

V. CFD Model

A. Domain and computational mesh

A CFD model was built in order to predict the exhaust gases in the combustion chamber from various fuels and validated through the experimental results previously described. This data were implemented in the compressible parallel finite volume-element solver ANSYS-FLUENT, which is able to handle hybrid grids to simulate the whole combustion process.

In a previous design process of an experimental dual burner [17] a preliminary model was built over a similar combustion chamber, but in this study, the full CHEMKIN® reaction solver [18] has been implemented and burner geometry redefined. Figure 6 a) shows the detail of the main section for the CFD mesh corresponding to the burner.

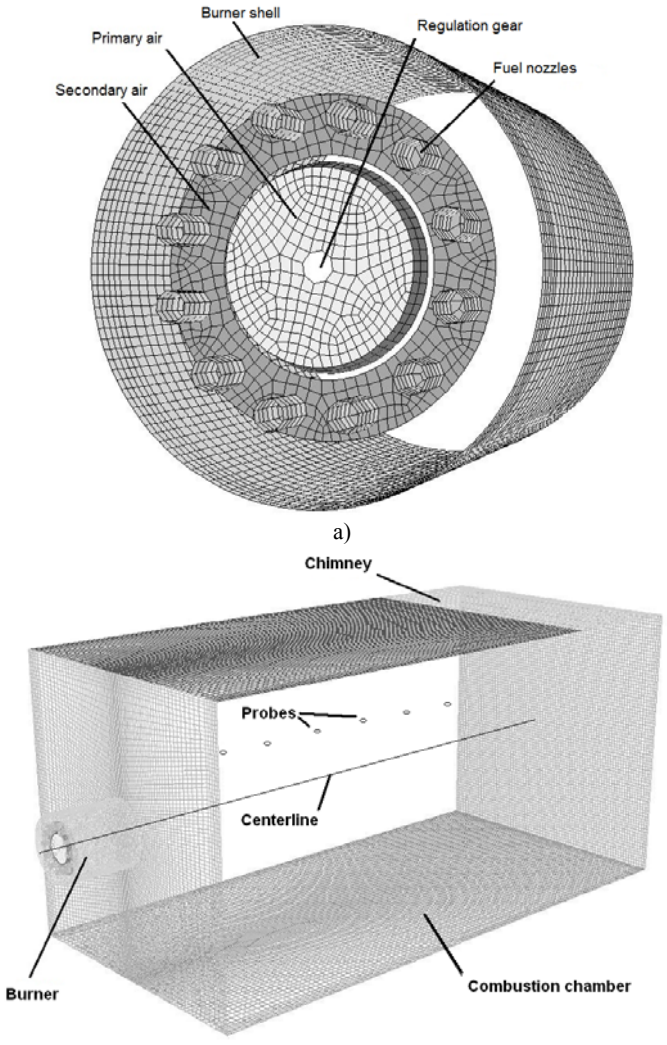

Fig. 6 a) Detail of the CFD burner mesh and b) Full model domain surface mesh with the different parts

The main air is supplied by a centrifugal fan and passes outside 12 uniformly-placed nozzles, where the fuel is finally injected through, producing the required air-fuel mixture while the initiating spark initiates the flame [19].

In Figure 6 b), the computational domain including burner and redefined combustion chamber are depicted. The outlet of the chamber can be clearly seen on the right side of the roof and the fuel nozzles are depicted inside the burner. The placement of the temperature probes for the experimental testing measurements are placed on one of the lateral walls, centred and separated 0.5m. as it is also depicted together with a virtual centreline in which further results will be based.

The grid was created using a powerful pre/processor code called ICEM CFD, and then the whole domain is fully discretized [20].

The size of the mesh was strictly determined by the treatment of the turbulence in the near-wall region. High quality numerical results for the wall boundary layer will only be obtained if the overall resolution of the boundary layer is sufficient [21].

The adjacent near-wall cell in the Non-Equilibrium Wall Functions model (NWF), "y_p" was determined depending on the choice of turbulent model used and was defined by the dimensionless term "y_p^+" [22]. This parameter can be calculated according to Eq. 25:

$$y_p^+ = \frac{y_p \cdot u_t}{v} \tag{25}$$

Where the friction velocity is defined by

$$u_t = \sqrt{\frac{\tau}{\rho}} \tag{26}$$

The logarithmic law is referenced to the pressure gradient in order to account for the phenomenon of moderate flow separation, so the centroid was placed between $30 \leq y_p^+ \leq 300$, which means a distance from the solid surface between: 0.25 mm $\leq y_p \leq$ 2.5 mm.

The smaller the size, the greater the number of cells and consequently an enhanced resolution can be achieved at added computational cost.

The discretization of the computational domain previously defined was realized with a maximum size of 0.9 mm, which is a reasonable estimation for a proper distribution of the centroid of the adjacent elements to the wall. 99.7 % of the cells in our model accomplish with $30 \leq y_p^+ \leq 300$.

In order to minimize numerical diffusion error, different grid sizes were analyzed, ensuring grid independence. The final mesh contained 4 10^6 cells, which resulted an easy to handle mesh, considered to be thin enough to capture the turbulence scales phenomena.

B. Boundary conditions

Once the discretization of the geometric volume was completed, the mesh is exported, into the main code (processor), where the boundary conditions would are set to complete the numerical model.

The boundary condition "mass flow inlet", for the fuel was selected because the corresponding value of the flow was available. Thus, the consumption of air was obtained by calculating the ratio "kg air/kg fuel" for combustion with an excess air of 10 % [23].

The condition of "outflow" for the outlet of the combustion chamber was adopted. It is appropriate where the exit flow is close to a fully developed condition, as the outflow boundary condition assumes a zero, normal gradient for all flow variables, except pressure.

The external walls of the burner were considered to be adiabatic, considering that the gas nozzle was inside the refractory of the fireplace. With the optical pyrometer, the maximum temperature that was reached on the lateral walls was measured.

To evaluate correctly the temperature of the walls, an average temperature was considered and two criteria were used. For the first criterion, the temperature of the exhaust gases was determined from the combustion chamber. This temperature depends on the power of heat given out by the burner and the heat exchange across the walls in the fireplace. For the second criterion, the heat across the walls for the thermal calculation was given by the manufacturer. To fit this value, modelling was carried out several times, imposing a temperature to the walls verifying always the values of the average temperature for the CEG and the flow of total heat evacuated through the walls.

C. Basic conservation equations

The conservation equations for mass and momentum were solved together with the energy and species conservation equations.

The equation for conservation of mass, or continuity equation, can be written as follows [24].

$$\frac{\partial \rho}{\partial t} + \nabla(\rho \vec{v}) = S_m \tag{27}$$

The source term is the mass added to the continuous phase from the dispersed second phase (e.g., due to vaporization of liquid droplets) and all the user-defined sources.

And the conservation of momentum in an inertial (non-accelerating) reference frame is given by:

$$\frac{\partial}{\partial t}(\rho \vec{v}) + \nabla(\rho \vec{v}\vec{v}) = -\nabla p + \nabla(\hat{\tau}) + \rho \vec{g} + \vec{F} \tag{28}$$

Where the stress tensor is given by

$$\hat{\tau} = \left[\mu\left(\nabla \vec{v} + \nabla \vec{v}^T\right) - \frac{2}{3}\nabla \cdot \vec{v} I \right] \tag{29}$$

The second term on the right hand side represents the effect of volume dilation.

Finally, the conservation of species is given by

$$\frac{\partial}{\partial t}(\rho m_i) + \nabla(\rho \vec{v} m_i) = \nabla(J_{i',i}) + S_i + R_i \tag{30}$$

Where the diffusive mass flow is defined by

$$J_{i',i} = -\rho D_{i',m} \nabla m_i - D_{i'}^T \frac{1}{T} \nabla T \tag{31}$$

Finally, the energy equation can be written

$$\frac{\partial}{\partial t}(\rho E) + \nabla(\vec{v}(\rho E + p)) = \nabla(k_e \nabla T - \sum_j h_j \vec{J}_j + (\hat{\tau} \cdot \vec{v})) + S_h \tag{32}$$

and the term E, is defined as,

$$E = h - \frac{p}{\rho} + \frac{v^2}{2} \tag{33}$$

D. Turbulence closure

Unfortunately no single turbulence model is universally accepted when dealing with all problem areas. The choice of turbulence model will depend on considerations such as the physics encompassed in the flow, the established practice for a specific class of problem and the level of accuracy required.

The realizable k-ε model in FLUENT has been finally adopted for this study, which is a variant of the standard k-ε model, including new formulation for the turbulent viscosity together with new transport equation for the dissipation rate ε [25]. It provides good predictions for adverse pressure gradient flows where near wall characteristics need to be resolved, while the computational cost is relatively low. The word "Realizable" actually implies that the model satisfies specific constraints on the Reynolds' stresses that make the model more consistent with the physics of turbulent flows and hence more accurate than the standard k- ε model [26]. Transport equations for k and ε are respectively as follows:

$$\frac{\partial}{\partial t}(\rho k) + \nabla(\rho k \vec{v}) = \nabla\left[\left(\mu + \frac{\mu_t}{\sigma_k}\right)\nabla k\right] + G_k + G_b - \rho \varepsilon - Y_M + S_k \tag{34}$$

$$\frac{\partial}{\partial t}(\rho \varepsilon) + \nabla(\rho \varepsilon \vec{v}) = \nabla\left[\left(\mu + \frac{\mu_t}{\sigma_\varepsilon}\right)\nabla \varepsilon\right] + C_1 \frac{\varepsilon}{k} G_{3\varepsilon} - \rho C_2 \frac{\varepsilon^2}{k} + S_\varepsilon \tag{35}$$

Where,

$$\mu_t = \rho C_\mu \frac{k^2}{\varepsilon} \tag{36}$$

$$G_k = \mu_{t,m}\left(\nabla \vec{v}_m + (\nabla \vec{v}_m)^T\right)\nabla \vec{v}_m \tag{37}$$

$$G_b = -g \cdot \frac{\mu_t}{\rho_m \cdot \sigma_h} \cdot \nabla \rho \tag{38}$$

This model makes the eddy-viscosity coefficient, Cv, dependent on the mean flow and turbulence parameters. The notion of variable Cv has been suggested by many authors and is well substantiated by experimental evidence. Note that in the realizable model, Cv can be shown to recover this standard

value of 0.09 for simple equilibrium flows. The rest of the model constants have been established to ensure that the model performs well for certain flows, such as,

$$C_1 = 1.44;\ C_2 = 1.9;\ \sigma_k = 1.0;\ \sigma_\varepsilon = 1.2 \tag{39}$$

E. Radiation closure

Radiative heat transfer was included because the radiant heat flux was high compared to the heat transfer rate due to convection or conduction. The radiative transfer equation (RTE) adopted for an absorbing, emitting, and scattering medium at position $\vec{r}$ in the direction $\vec{s}$, is:

$$\frac{dI(\vec{r},\vec{s})}{ds} + (a+\sigma_s)\cdot I(\vec{r},\vec{s}) = a\cdot n^2\cdot\frac{\sigma\cdot T^4}{\pi} + \frac{\sigma_s}{4\pi}\int_0^{4\pi} I(\vec{r},\vec{s})\cdot\Phi(\vec{s},\vec{s}')\,d\Omega \tag{40}$$

The weighted-sum-of-gray-gases model (WSGG) for computation of a variable absorption coefficient is provided. The net radiative heat flux at flow inlets and outlets is computed in the same manner as at the walls, as described above. The *P-1* radiation model is based on the expansion of the radiation intensity into an orthogonal series of spherical harmonics [27]. The following equation is obtained for the radiation flux:

$$q_r = \frac{1}{3\cdot(a+\sigma_s) - C\cdot\sigma_s}\cdot\nabla G \tag{41}$$

The transport equation for G is:

$$\nabla\left(\left[\frac{1}{3\cdot(a+\sigma_s) - C\cdot\sigma_s}\right]\nabla G\right) - a\cdot G + 4\cdot a\cdot\sigma\cdot T^4 = S_G \tag{42}$$

It has been assumed that the emissivity of all flow inlets and outlets is 1.0 (black body absorption). For a gray, absorbing, emitting, and scattering medium containing absorbing, emitting, and scattering particles, the transport equation for the incident radiation can be written as:

$$\nabla(\Gamma\nabla G) + 4\pi\cdot\left(a\cdot\frac{\sigma\cdot T^4}{\pi} + E_P\right) - (a+a_P)\cdot G = 0 \tag{43}$$

Where,

$$\Gamma = \frac{1}{3(a+a_P+\sigma_P)} \tag{44}$$

$$\sigma_P = \lim_{V\to 0}\sum_{n=1}^{N}(1-f_{pn})\cdot(1-\in_{pn})\cdot\frac{A_{pn}}{V} \tag{45}$$

$$E_P = \lim_{V\to 0}\sum_{n=1}^{N}\in_{pn}\cdot A_{pn}\cdot\frac{\sigma\cdot T_{pn}^4}{\pi V} \tag{46}$$

$$a_P = \lim_{V\to 0}\sum_{n=1}^{N}\in_{pn}\cdot\frac{A_{pn}}{V} \tag{47}$$

$$A_{pn} = \frac{\pi\cdot d_{pn}^2}{4} \tag{48}$$

So, finally, heat sources (sinks) due to particle radiation are included in the energy equation as follows:

$$-\nabla\cdot q_r = -4\pi\cdot\left(a\cdot\frac{\sigma\cdot T^4}{\pi} + E_P\right) + (a+a_P)\cdot G \tag{49}$$

F. Combustion closure

The above mentioned model, considered the incorporation of improved UDF (user defined functions) under the ANSYS-FLUENT solver of which combustion model obeys to a probability density function (PDF). The laminar flamelet approach, modelled a turbulent flame brush as an ensemble of discrete, steady, laminar flames, called flamelets [28]. They were assumed to have the same structure as laminar flames in simple configurations, and were obtained by experiments or calculations. Using detailed chemical mechanisms, laminar opposed-flow diffusion flamelets for non-premixed combustion can be calculated.

The advantage of the laminar flamelet approach was that realistic chemical kinetic effects could be incorporated into turbulent flames. The chemistry could then be pre-processed and tabulated, minimizing computation substantially. However, the laminar flamelet model was limited to modelling combustion with relatively fast chemistry [29]. The flame was assumed to respond instantaneously to the aerodynamic strain, and thus the model was unable to capture deep non-equilibrium effects such as ignition, extinction, and slow chemistry.

The conserved scalar model was interpreted as the most basic flamelet structure. The coupling between non-equilibrium chemistry and turbulence was achieved by the statistical description of two parameters: the mixture fraction (f) and the instantaneous scalar dissipation rate (χ). Under the assumption of equal diffusivities, a coordinate-free formulation of the flamelet structure was considered [30]. The hypothesis of statistical independence of these two parameters was also discussed.

On the one hand, the mixture fraction definition can be understood in relation to common measures of reacting systems [31]. Consider a simple combustion system involving a fuel stream [32], an oxidant stream, and a product stream symbolically represented at stoichiometric conditions as:

$$F_s + r\cdot O_s \rightarrow (1+r)\cdot P_s \tag{50}$$

Denoting the equivalence ratio as:

$$\phi = \frac{(fuel/air)_{actual}}{(fuel/air)_{stoichiometric}} \tag{51}$$

So, the reaction in equation (50), under more general mixture conditions, can then be written as:

$$\phi \cdot F_s + r \cdot O_s \rightarrow (\phi + r) \cdot P_s \quad (52)$$

Looking at the left side of this equation, the mixture fraction for the system as a whole can then be deduced as:

$$f = \frac{\phi}{\phi + r} \quad (53)$$

Equation (53) allows the computation of the mixture fraction at stoichiometric conditions (ϕ = 1) or at fuel-rich conditions (ϕ >1), or fuel-lean conditions (ϕ <1).

On the other hand, the scalar dissipation rate is defined as:

$$\chi = 2D \cdot |\nabla f|^2 \quad (54)$$

For adiabatic systems, the density-weighted mean species mass fractions and temperature in the turbulent flame can be determined as:

$$\bar{\phi}_{m,T} = \iint \phi_{m,T}(f, \chi_{st}) \cdot p(f, \chi_{st}) \cdot df \cdot d\chi_{st} \quad (55)$$

where:

$$\chi_{st} = \frac{a_s \cdot exp\left[-2 \cdot \left[erfc^{-1}(2 f_{st})\right]^2\right]}{\pi} \quad (56)$$

When introducing fuel to an oxidant, spontaneous ignition does not occur unless the temperature of the mixture exceeds the activation energy threshold required to maintain combustion. It is necessary to supply an ignition source to initiate combustion. This source may be a heated surface or inlet mass flow that heats the gas mixture above the required ignition temperature. Often, however, it is the equivalent of a spark: an initial solution state that causes combustion to proceed into a region of the CFD model that contains a sufficient fuel/air mixture for ignition to occur.

The temperature-dependent portion of the rate expression contains an exponential, which is computationally expensive to evaluate. To facilitate a more computationally efficient solution algorithm, CHEMKIN® [18] provides additional subroutines that either provide the temperature-dependent rate coefficients or, given these rate coefficients, return the species' net rates of production.

In addition to chemically reacting flow applications, it includes an Equilibrium Reactor model. This model allows users to determine the chemical state of a mixture under equilibrium conditions. It can be used to determine phase equilibrium, between gas and condensed phases, as well as chemical equilibrium.

Gas-phase reactions describe interactions and conversions between gas-phase species. Each species in a reaction must be associated with thermodynamic data which are used to calculate equilibrium constants and reverse-rate coefficients for the reaction [33]. Consider elementary reversible (or irreversible) reactions involving the chemical species that can be represented in the general form:

$$\sum_{k=1}^{K} \upsilon'_{ki} \cdot \chi_k \quad \Leftrightarrow \quad \sum_{k=1}^{K} \upsilon''_{ki} \cdot \chi_k \quad (i = 1,...,I) \quad (57)$$

The production rate of the k th species can be written as a summation of the rate of-progress variables for all reactions involving the k th species:

$$\dot{\omega}_k = \sum_{i=1}^{I} \upsilon_{ki} \cdot q_i \quad (k = 1,...,K) \quad (58)$$

The "third body" is required for the reaction to proceed; this is often the case in dissociation or recombination reactions. The concentration of the effective third body must appear in the expression for the rate-of-progress variable as:

$$q_i = \left(\sum_{k=1}^{K} (a_{ki}) \cdot [X_k]\right) \cdot \left(k_{fi} \prod_{k=1}^{K} [X_k]^{\upsilon'_{ki}} - k_{ri} \prod_{k=1}^{K} [X_k]^{\upsilon''_{ki}}\right) \quad (59)$$

It was assumed that heat gain/loss to the system would have negligible effect on the species mass fractions, and adiabatic mass fractions were used.

G. NOx post-processing

The post process NO_x model includes: thermal, prompt, fuel, and intermediate NO_2 routes.

- *Thermal route:*

This is determined by a set of highly temperature-dependent chemical reactions known as the extended "Zeldovich mechanism" [34]. The principal reactions governing the formation of thermal NO_x from molecular nitrogen are as follows:

$$\begin{aligned} &O + N_2 \Leftrightarrow N + NO \\ &N + O_2 \Leftrightarrow O + NO \\ &N + OH \Leftrightarrow H + NO \end{aligned} \quad (60)$$

Hence, the NO source term due to thermal NO_x mechanisms is:

$$S_{Thermal,NO} = M_{w,NO} \cdot \frac{d[NO]_T}{dt} \quad (61)$$

- *Prompt route:*

The presence of a second mechanism leading to NO_x formation was first identified by Fennimore [35] and was termed "prompt NO_x". There is good evidence that it can be significantly performed in some combustion environments, such as in low-temperature, fuel-rich conditions, and in situations where residence times are short. Surface burners or staged combustion systems, can create such conditions [36].

At present the prompt NO_x contribution to total NO_x from stationary combustors is small. However, as NO_x emissions are reduced to very low levels by employing new strategies (burner design or furnace geometry modification as it can be considered for this study), the relative importance of the

prompt NO_x can be expected to increase. The route now accepted is as follows:

$$\begin{aligned} &CH + N_2 \Leftrightarrow HCN + N \\ &N + O_2 \Leftrightarrow O + NO \\ &HCN + OH \Leftrightarrow CN + H_2O \\ &CN + O_2 \Leftrightarrow NO + CO \\ &CH_2 + N_2 \Leftrightarrow HCN + NH \\ &HCN + N \Leftrightarrow N_2 + ... \end{aligned} \quad (62)$$

In other studies [30], comparison of probability density distributions for the location of the peak NO_x with those obtained for the peak CH have shown close correspondence, indicating that the majority of the NO_x at the flame base is prompt NO_x formed by the CH reaction [37].

The NO source term due to prompt NO_x mechanisms is:

$$S_{prompt,NO} = M_{w,NO} \cdot \frac{d[NO]_{Pr}}{dt} \quad (63)$$

- *Fuel route:*

It is well known that nitrogen-containing organic compounds present in liquid or solid fossil fuel can contribute to the total NO_x emissions during the combustion process. This fuel nitrogen is a particularly important source of nitrogen oxide emissions for residual fuel oil and coal, which typically contain *0.3-2 %* nitrogen by weight. Studies have shown that most of the nitrogen in heavy fuel oils is in the form of heterocycles and of significance are heterocyclic ring structures such as pyridine, quinoline, and amine type [38].

The extent of conversion of fuel nitrogen to NO_x was dependent on the local combustion characteristics and the initial concentration of nitrogen-bound compounds. Fuel-bound nitrogen-containing compounds were released into the gas phase when the fuel droplets or particles were heated during the devolatilization stage. From the thermal decomposition of these compounds in the reaction zone, radicals such as HCN, NH_3, N, CN, and NH were formed and converted to NO_x. These free radicals are subject to a double competitive reaction path [39]. Other investigations have shown that hydrogen cyanide appears to be the principal product if fuel nitrogen is present in aromatic or cyclic form [40]. Although the route leading to fuel NO_x formation and destruction is still not completely understood, different investigators [41] seem to agree on a simplified model such as:

$$FUEL\ N_2 \rightarrow \begin{matrix} N_2 \\ HCN \end{matrix} \ intermediate \ \ or \begin{cases} \xrightarrow{(1)O_2} NO \\ \xrightarrow{(2)NO} N_2 \end{cases} \quad (64)$$

The source terms in the transport equations can be written as follows:

$$\begin{aligned} &S_{HCN} = S_{pl,HCN} + S_{HCN-1} + S_{HCN-2} \\ &S_{NO} = S_{NO-1} + S_{NO-2} \end{aligned} \quad (65)$$

- *Intermediate N_2O route:*

Nitrogen enters combustion systems mainly as a component of the combustion and dilution air. Under favorable conditions, which include elevated pressure and oxygen-rich conditions, this intermediate mechanism can contribute as much as 90 % of the NO_x formed during combustion. This makes it particularly important in equipments such as gas turbines and compression-ignition engines. As these devices are operated at increasingly low temperatures to prevent NO_x formation through the thermal NO_x mechanism, the relative importance of the N_2O-intermediate mechanism is increasing [42].

The simplest form of the mechanism takes into account two reversible elementary reactions:

$$\begin{aligned} &N_2 + O + M \Leftrightarrow N_2O + M \\ &N_2O + O \Leftrightarrow 2NO \end{aligned} \quad (66)$$

Here, M is a general "third body". As the first reaction involves third bodies, the mechanism is favoured at elevated pressures. Both reactions involve oxygen radical, which makes the mechanism favoured in oxygen-rich conditions. Although it is not always justified, it is often assumed that the O atoms originate solely from the dissociation of molecular oxygen.

VI. Results and Discussion

A. Experimental results from the combustion chamber

The boiler was loaded about one hour before the starting of the tests in order to ensure stability, especially for several parameters such as: pressure, temperature, and flow of both gases and water.

The different instruments were checked in order to verify the stability of the process. The parameters were considered to be steady when the variation between them did not exceed a range of 5 % in every measurement process.

Once stability was achieved, the input of data started. All the tests and measurements were carried out with the experimental burner in automatic mode (working conditions of the burner were defined automatically, according to heat consumption) as well as manual alternative selection of low and high flame process monitoring respectively [43].

Results obtained in the combustion of NG and BG respectively is summarized in Table 7. The combustor performance with both fuels is similar, being obtained with comparable values of temperature rise, combustion efficiency and CO emissions.

B. Validation

Experimental values measured with the previously mentioned facility at the exit of the combustion chamber and the results obtained with the CFD model were summarised in Table 8 for natural gas and bio-gas respectively which seem to be the best options. A significant agreement is achieved between CFD and experimental results showing that the procedure can be considered fully validated. Observe that experimental losses for both cases (*) based on data provided by direct temperature measurements over the walls were calculated.

Table 7. Measured values in the combustion chamber.

	NG	BG
Environment:		
• **Dry bulb temperature (K)**	296.00	297.00
• **Barometric pressure (Pa)**	101,329.00	101,330.00
• **Relative humidity (%)**	78.00	79.00
Chimney:		
• **CO (ppm)**	3.60	4.36
• **CO_2 (%)**	10.90	14.90
• **O_2 (%)**	2.00	1.00
• **Outlet temperature (K)**	512.00	505.00
Chamber:		
• **CO_2 (%)**	10.60	14.60
• **O_2 (%)**	2.10	2.40
• **Outlet temperature (K)**	1,352.00	1,343.00
• **Máx. temperature (K)**	2,138.00	2,159.00
Water:		
• **Flow (kg s^{-1})**	12.20	12.20
• **Inlet temperature (K)**	388.20	389.10
• **Outlet temperature (K)**	417.00	419.00
• **Total pressure (Pa)**	1,084.10	1,088.20
Fuel:		
• **Flow (kg s^{-1})**	0.03	0.03
• **Inlet temperature (K)**	295.00	295.00
• **Relative pressure (Pa)**	6,754.10	6,758.20

Table 8. Validation of the CFD model.

	NG		BG	
	Exp	**CFD**	**Exp**	**CFD**
Q_b (W)	545,221 (*)	544,970	555,546 (*)	554,908
T_{avg} (K)	1,352.00	1,360.41	1,343.00	1,350.32
T_{max} (K)	2,138.00	2,169.00	2,159.00	2,180.00
CO (ppm)	3.60	3.63	4.36	4.69
NO (ppm)	42	43	44	46
NO_2 (ppm)	0.6	1	1.6	2

A small difference in the maximum combustion temperature was expected, because it is well known that the combustion model tends to over-predict such values of temperature. As a consequence, the temperature of the combustion exhaust gases from the combustion chamber is obviously slightly lower than this given value [44].

Figure 7 a) shows the average temperature along the centerline of the combustion chamber in a comparative test for experimental values and CFD outcomes for NG, whereas in figure 7 b) the same are depicted for BG, showing in both cases a good agreement both in values and distribution.

To quantify properly the variations between the measured data and CFD outcomes, the square of the Pearson product moment correlation coefficient (R^2) is calculated according to:

$$R^2 = \left(\frac{\sum_{t=1,n}(X_t - \bar{X})(M_t - \bar{M})}{\sqrt{\sum_{t=1,n}(X_t - \bar{X})^2 \sum_{t=1,n}(M_t - \bar{M})^2}} \right)^2 \quad (67)$$

This can be visualized graphically in Figure 8. The values obtained are admissible for both fuels tested.

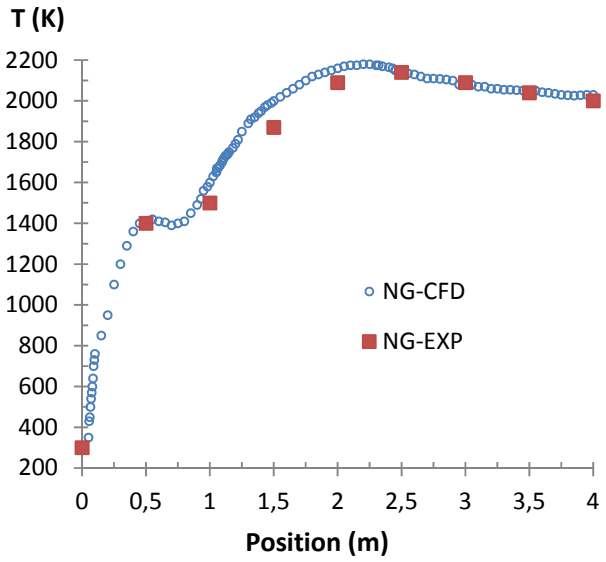

a)

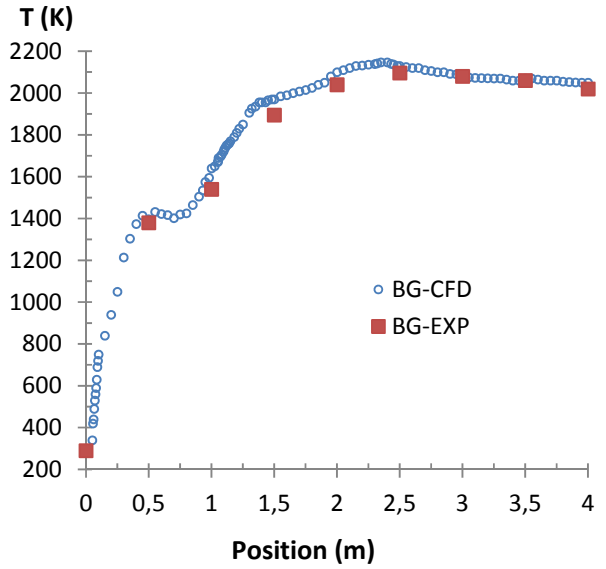

b)

Fig. 7. Experimental and CFD temperatures (K) along the centerline of the chamber, a) NG; b) BG.

In Figure 9, flame speed vs. equivalence ratio is depicted in the form of a comparative study (at normalized conditions of 298K and 1 atm) between similar works carried out by different researchers when burning NG [45 - 48]. For our model, in the primary zone, the value of $\phi = 1.4$ corresponds to a speed of approximately 0.20 m/s which is relatively low, while in the secondary zone $\phi = 0.7$ corresponds to a speed of 0.14 m/s.

Strong differences between both zones are shown. Targets demonstrated that our model best matches fame speeds at different conditions, which finally allow us to validate the structure of the temperature profiles adopted for our model, improving this way the above mentioned predictions and others [49].

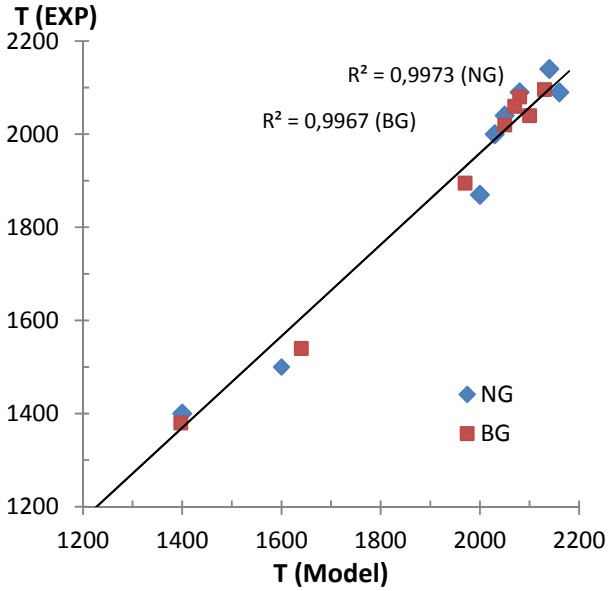

Fig. 8. Error treatment.

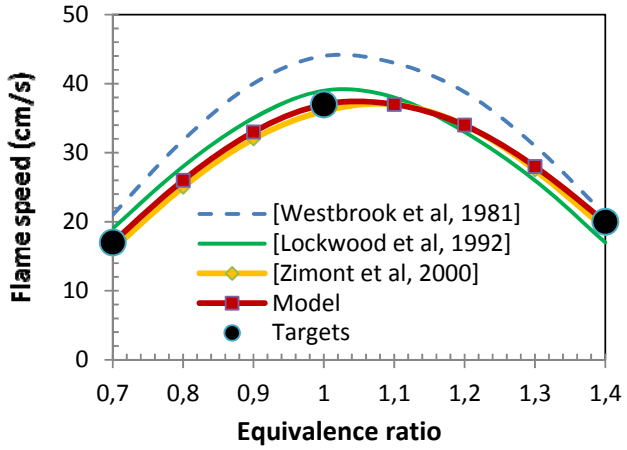

Fig. 9. Different flame speeds (cm s^{-1}) at 298K and 1 atm for NG.

C. CFD outcomes

Results are shown over the symmetry plane of the combustion chamber for the two fuels, in order to visualize the differences observed.

Figure 10 shows the contours of total temperature (K), addressing the flame temperature. NG offers lower temperatures than BG.

Fig. 11 shows the contours of CO (ppm) over the symmetry plane of the combustion chamber for two different fuels such as NG and BG, addressing the quality of the combustion.

Contours of CO are revealed following the flame shape, as expected, especially at the end of the chamber where finally it almost becomes exhausted especially regarding the combustion of the natural gas. A higher amount of CO traces has revealed anyway in the case of BG as expected from the experimental values measured at the exit of the chamber. Anyway these values are rather similar in both cases.

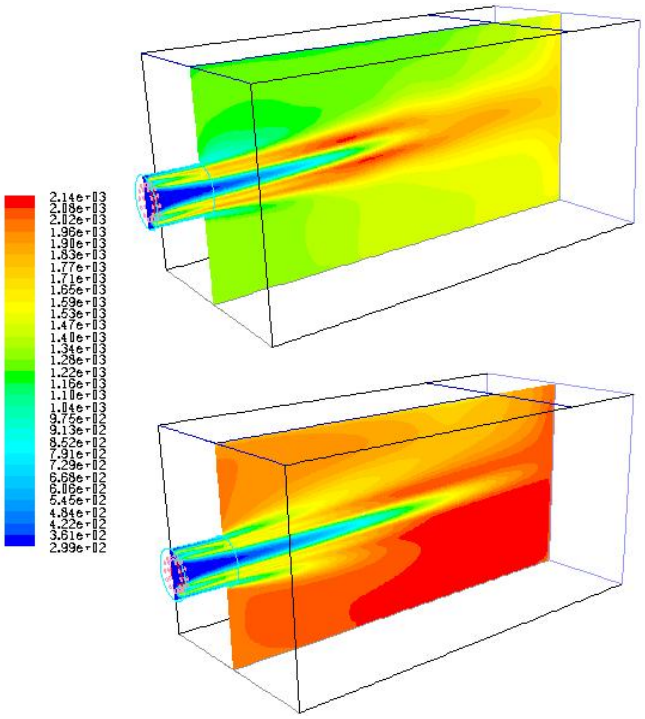

Fig. 10. T (K) inside the chamber, up NG; down BG.

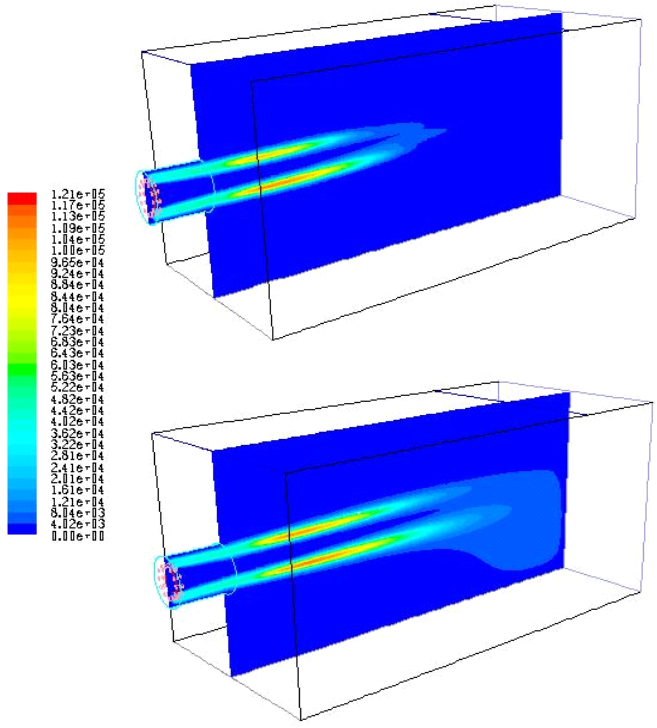

Fig. 11. CO (ppm) inside the chamber, up NG; down BG.

Figure 12 shows the contours of CO_2 (ppm) over the symmetry plane of the combustion chamber for the same two fuels, NG (up) and BG (down). Differences in combustion between the two fuels are not evident as CO_2 concentrations are somewhat distributed in a different way.

Figure 13 shows the contours of NO (ppm) over the symmetry plane of the combustion chamber for the same two fuels, NG (up) and BG (down).

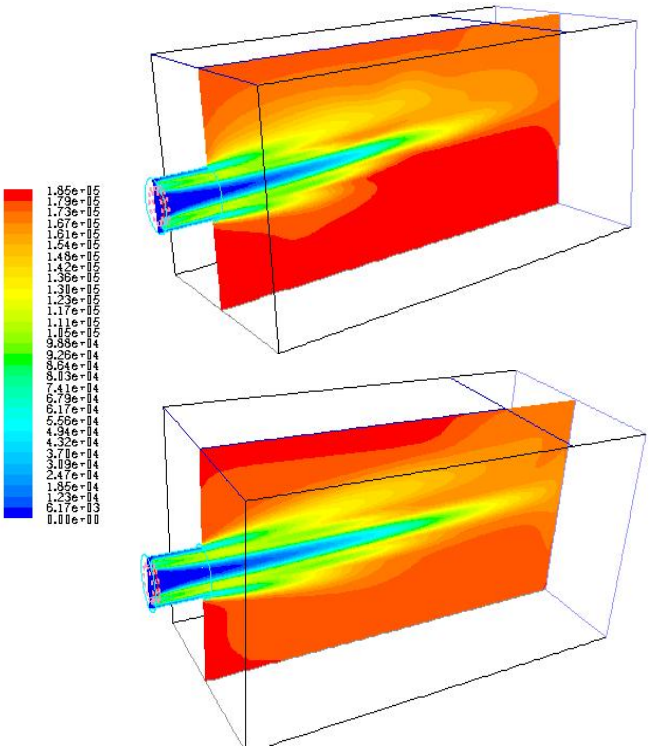

Fig. 12. CO_2 (ppm) inside the chamber, up NG; down BG.

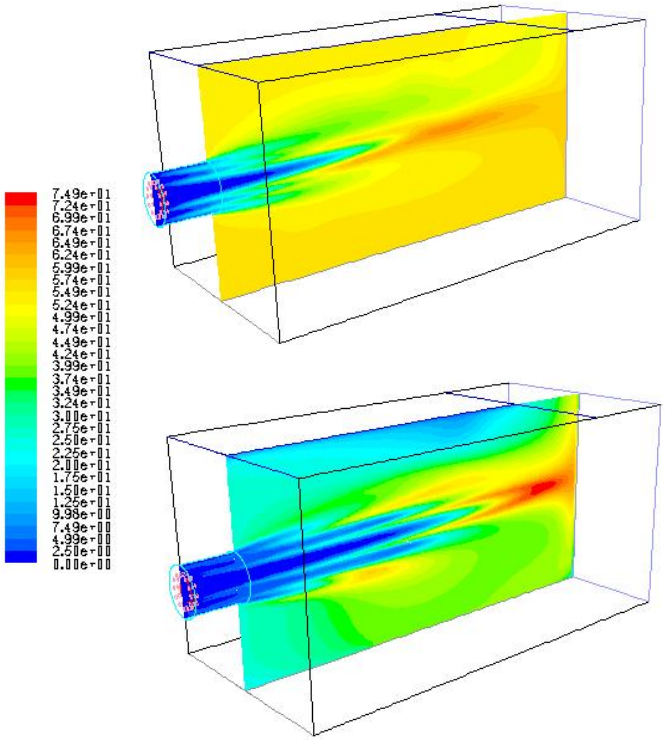

Fig. 13. NO (ppm) inside the chamber, up NG; down BG

Contours of NO are clearly influenced by temperature [50]. In this case the differences for both fuels are evident, resulting in a bigger amount of NO emissions for NG.

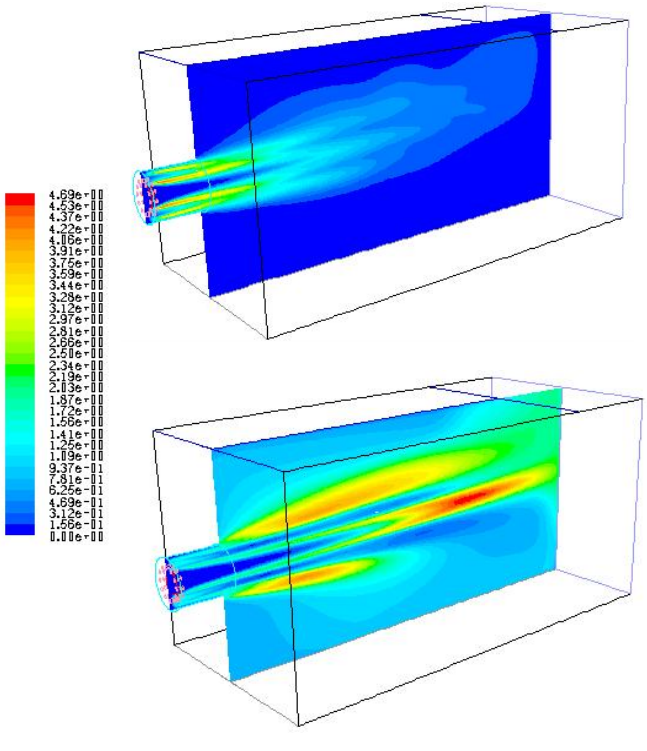

Fig. 14. NO_2 (ppm) inside the chamber, up NG; down BG

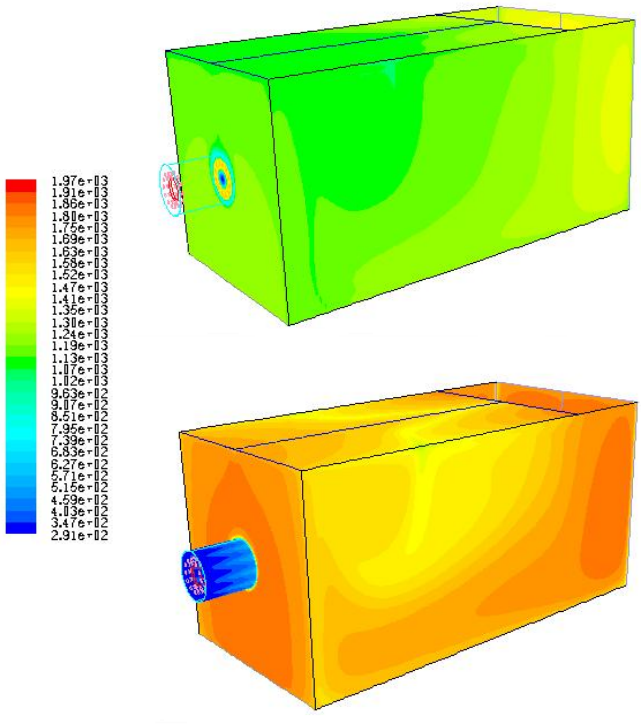

Fig. 15. Surface temp. (K) inside the chamber, up NG; down BG

Figure 14 shows the contours of NO_2 (ppm) over the symmetry plane of the combustion chamber. In this case, emissions for NG are almost annulled [51] at the chimney whereas for BG, values are greater.

The effect of the heat transfer process from the CEG to the walls over the whole combustion chamber was carefully evaluated through Figure 15, as was previously shown in Table 8 for validation purposes. Surface temperatures for BG are simply greater, showing bigger heat losses through walls.

Finally, a comparative test was performed for both fuels. Figure 16 a) depicts the Mean mixture fraction [52] whereas in Figure 16 b) shows the specific heat at constant pressure Cp, Both figures are reported along a centerline of the chamber, showing similar values for both fuels but highlighting bigger amounts for NG.

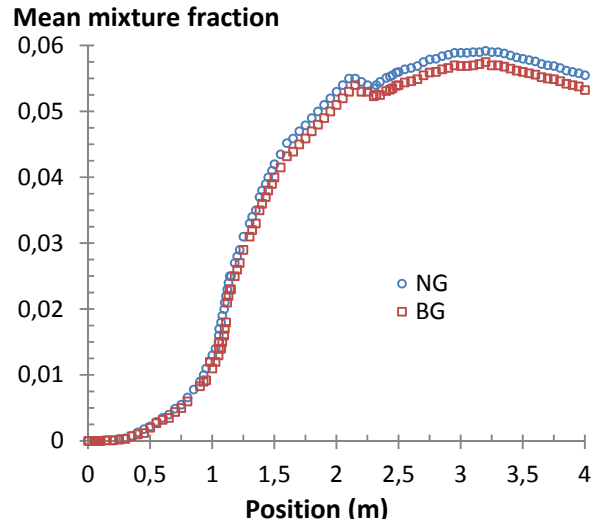

a)

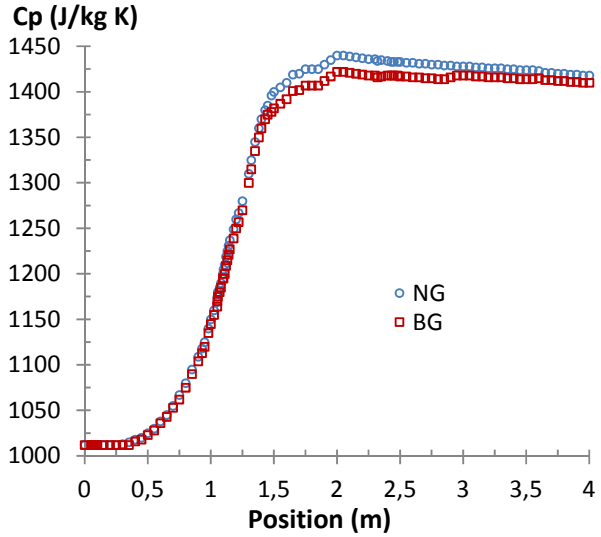

b)

Fig. 16. Comparative test for NG and BG along a centerline of the chamber, a) Mean mixture fraction and b) Cp

VII. Conclusions

This paper presents a complete methodology for the evaluation process of re-converting thermal plants firing fuel-oil into alternative fuels which are nowadays becoming a credible alternative for gas turbines when fossil fuels are scarce or expensive. Two alternatives were studied, such as natural gas and a particular biomass derived fuel obtained in fluidized beds. A key factor of such fuel replacement is to ensure that global efficiency of the whole plant is kept constant, so a rigorous study for the evaluation of such efficiency according to the fuel burned was presented here, prior to proceeding with any fuel replacement.

On the one hand, the evaluation of the boiler and global efficiencies associated to the burning of fuel oil (both standard type and low sulphur index), natural gas and biomass derived gas respectively (regarding both Gross and Lower Calorific Values) including an exhaustive definition of the "losses and credit factor terms" has been carried out here. An innovative improvement on the definition of the "difficult evaluation losses term", has been highlighted here, obtaining for such fuels, values really close although natural gas presents slightly higher figures in the range 0.42 - 1%. Anyway, the considerable amount of ashes present in the matrix of these fuels would represent a decreasing on their respective real thermal efficiencies comparing with the values calculated here.

On the other hand, for the characterization of the fuel behaviour in terms of pollution and performance, a detailed study through Computational Fluid Dynamics was presented, which has revealed as a powerful tool. The final improved models implement the CHEMKIN® code and have been widely validated throughout a fully monitored experimental facility showing a significant agreement with the CFD outcomes. This means a considerable improvement in relation to previous results, due on the one hand to the implementation of the great number of equations fully solved now in the combustion process, and on the other hand, to the use of improved User Defined Functions (UDF) defining faithfully the behavior of fluids properties involved. Natural gas once again reaches better values regarding environmental pollution with regard to the bio gas, both CO and NOx.

Detailed information about the axial flame temperature was also obtained by performing several thermocouple traverse measurements on the experimental facility which has been useful for the characterization and further validation of the heat transfer across the walls for the different fuels tested, carried out through CFD. In general terms, the range of efficient operation when burning biogas decreases compared with the operation with standard fuels.

Finally, this study brings the possibility of analyzing and testing other fuels of interest in the future in a small scale over this scaled combustion chamber, which could provide valuable comparative information and further insight.

Acknowledgment

Authors deeply thank the control staff of the thermal power plant of reference for their help, support and assistance on the test experiments and also for their suggestions in the elaboration of this manuscript inside OPCOFLUID project.

NOMENCLATURE

a	Gas absorption coefficient.
a_P	Equivalent absorption coefficient.
A	Amount of structural water in the fuel matrix.
A_{pn}	Projected area of the particle *n*.
BG	Gas derived from biomass (Bio-Gas).
CEG	Combustion exhausts gases.
CFD	Computational Fluid Dynamics.
CO_2	Carbon dioxide.
Cp	Specific heat capacity at constant pressure (kJ kg^{-1} K^{-1})
Cv	Eddy-viscosity coefficient.
d_{pn}	Diameter of the particle *n*.
DE	Difficult evaluation losses term (%).
$D_{i'}^{T}$	Soret diffusion coefficient.
$erfc^{-1}$	Inverse complementary error function.
E	Energy term.
E_p	Full load electrical consumption of the pumps (kJ h^{-1}).
E_P	Equivalent emission of particles.
f	Mixture fraction.
f_{st}	Stoichiometric mixture fraction.
f_{pn}	Scattering factor associated with the particle n.
F_s	Fuel stream (generic).
$\vec{F}$	External body forces.
fCr	Credit factor (kJ/kg fuel).
FO	Fuel Oil.
GCV	Gross calorific value (kJ/kg fuel).
G	Incident radiation term.
G_k	Production of turbulence kinetic energy due to gradients.
G_b	Production of turbulence kinetic energy due to buoyancy.
h	Specific enthalpy (KJ kg^{-1})
H	Amount of hygroscopic water in the fuel matrix.
$[H_2O]$	Water mass fraction.
I	Unit tensor.
I	Radiation intensity.
$J_{i',i}$	Diffusive mass flow
$\vec{j}_j$	Diffusion flux of species
k	Turbulent kinetic energy term.
k_e	Effective conductivity.
LCV	Lower calorific value (kJ/kg fuel).
LSI	Low Sulphur Index.
M	A general third body.
M_w	Molecular weight of NO (kg $[gmol]^{-1}$).
m	Mass (kg).
$\dot{m}$	Mass flow (kg h^{-1}).
n	Refractive index.
N	Number of surfaces in the boiler.
NG	Natural gas.
NWF	Non-Equilibrium Wall Functions model.
O_s	Oxidant stream (generic).
P_s	Product stream (generic).
p	Static pressure (bar).
P	Losses (kJ/kg fuel).
PDF	Probability Density Fucntion
ppm	Particles per million.
PFBC	Pressurized Fluidized Bed Combustion.
q_i	Rate of progress of the i *th* reaction (mol cm^{-2} s^{-1}).
q_r	Radiation flux.
Q	Total heat power supplied (W).
RTE	Radiative Transfer Equation.
R_i	Net rate of production of species i.
R_{cf}	= Mean limiting reaction rate of fuel (kg m-3 s-1).
r	Latent heat of vaporization for the water (kJ kg^{-1}).
r	Air-to-fuel ratio on a mass basis.
$\vec{r}$	Position vector.
$\vec{s}$	Direction vector.
$\vec{s}'$	Scattering direction vector.
S	Total surface (m^2).
S_{ct}	Turbulent Schmidt number.
S_i	Source term of mass.
S_h	Source term of energy.
S_G	User-defined radiation source.
S_{HCN}	Consumption rates of *HCN* (kg m^{-3} s^{-1}).
$S_{pl,HCN}$	Source of HCN (kg m^{-3} s^{-1}).
T	Gas local temperature (K).
T_k	Temperature of the kth species (K).
u’	Ratio of the root-mean-square of the velocity fluctuations.
u_t	Friction velocity (m s^{-1}).
UDF	User Defined Function.
$\vec{v}$	Velocity (m s^{-1}).
v	Air velocity (ft s^{-1}).
V	Volume (Nm^3).
WSGG	Weighted-sum-of-gray-gases model.
x	Absolute humidity (kg water/kg dry air)
$[X_k]$	Molar concentration of the kth species (mol m^{-3}).
Y_j	Local species mass fraction.
Y_M	Contribution of the fluctuating dilatation to the dissipation.
$Y_{N,fuel}$	Mass fraction of nitrogen in the fuel.
y_p	Size of the adjacent near-wall cell (mm).
y_p^+	Adimensional sub layer thickness.

Greek symbols

ρ	Density.
ρg	Gravitational body forces.
υ_k	Thermal Diffusion velocity of the *k*th species (cm s^{-1}).
η	Efficiency.
ε	Boiler external walls emissivity (0.95)
ε	Dissipation Rate term of the transport equation (m^2 s^{-3}).
Σ	Sum.
Δ	Delta (increment).
∇	Derivative.
Φ	Phase function.
Ω’	Solid angle.
$\bar{\tau}$	Stress tensor.
μ	Molecular viscosity.
μ_t	Turbulent viscosity.
κ	Von Kármán constant (0.4187).
σ	Stefan-Boltzman constant (5.669 10^{-8} W m^{-2} K^{-4}).
σ_S	Scattering coefficient.
σ_k, σ_ε	Turbulent Prandtl numbers for k and ε respectively.
σ_P	Equivalent particle scattering factor.
σ_S	Scattering coefficient.
Γ	Radiation quantity.
χ	Scalar dissipation rate.
χ_{st}	Stoichiometric scalar dissipation rate.
ϕ	Equivalence ratio.
$\bar{\phi}_{m,T}$	Density-weighted mean species mass fractions.

Subscripts

a	Related to air comburent.
avg	Related to average.
b	Related to boiler.
bw	Related to boiler walls.
c	Related to cycle.
C	related to convection.
CO	Related to carbon monoxide.
CR	Related to convection-radiation.
da	Related to dry air.
de	Related to difficult evaluation losses.
dg	Related to dry gases.
ext	Related to external air conditions.
G	Related to global.
heat	Related to heaters.
H2	Related to hydrogen.
lat	Related to latent.
m	Related to mass.
p	Related to recirculation pumps.
R	Related to radiation.
sat	Related to saturated vapour.
v	Related to volume.
vap	Related to water vapour.
wa	Related to air moisture.
wf	Related to fuel moisture.

REFERENCES

[1] J.M. Blanco, L. Remaki, F. Peña, Environmental impact test in thermal power plants; experimental and CFD evaluation of burning alternative fuels, Proceedings International conference on Environmental Science and Geoscience (ESG 2015), Vienna, Austria, 2015, pp. 11-18.

[2] J.M. Beér, Combustion technology developments in power generation in response to environmental challenges, Prog. Energy Combust. Sci., **26**, 2001, pp. 301-327.

[3] I. Gökalp, E. Lebas, Alternative fuels for industrial gas turbines (AFTUR), Appl. Therm. Eng., 24, 2004, pp. 1655-1663.

[4] M. Molière, E. Panarotto, M. Aboujaib, Gas Turbines in Alternative Fuel Applications: Biodiesel Field Test, ASME Turbo Expo'07, Montreal, Canada, 2007, pp. 1235-1239.

[5] A. Tolón-Becerra, X. Lastra-Bravo, F. Bienvenido-Bárcena, Proposal for territorial distribution of the EU 2020 political renewable energy goal, Renew. Energy, 36/8, 2011, pp. 2067-2077**.**

[6] Y. Huang, D. McIlveen-Wright, S. Rezvani, Y.D. Wang, N. Hewitt, B.C. Williams, Biomass co-firing in a pressurized fluidized bed combustion (PFBC) combined cycle power plant: A techno-environmental assessment based on computational simulations, *Fuel Procc. Technol.*, 87/10, 2006, pp. 927-934.

[7] N. Smirnov, Y. Phylippov,V. Nikitin, M. Silnikov, Modeling of combustion in engines fed by hydrogen, *WSEAS Transactions on fluid mechanics*, 9, 2014, pp. 154-167.

[8] M. Acaro, D. Aksoy, The cultivation and energy balance of Miscanthus giganteus production in Turkey, Biomass and bioenergy, 29/1, 2005, pp. 42-48.

[9] J.M. Blanco, F. Peña, Analytical study of the effects of the clogging of a mechanical precipitator unit in air preheaters in a high-performance thermoelectric power plant based on available data. ASME J. Eng. for Gas Turbines and Power, 130(2), 2008, pp. 22001-22007.

[10] D. Cialdea, L. Mastronardi, Renewable Energy Resources and their impact on Rural Landscape, *WSEAS Transactions on environment and development*, 10, 2014, pp. 423-433.

[11] M. Moliere, Expanding fuel flexibility of gas turbines, Journal of Power and Energy, 219/2, 2005, pp. 109-119.

[12] J.M. Blanco, F. Mendía, F. Peña, Comparative analysis of CO_2 and SO_2 emissions between combined and conventional cycles with natural gas and fuel oil consumption over the Spanish thermal power plants, Fuel, 85, 2006, pp. 1280-1285.

[13] J. Matthew, R. De Kam, M. Vance, D.G. Tiffany, Biomass Integrated Gasification Combined Cycle for heat and power at ethanol plants, Energy Convers. Management, 50/7, 2009, pp. 1682-1690.

[14] S.X. Zhou, Z.P. Song, On evaluation reference of energy utilizations, Journal Eng. Thermophysics, 29/8, 2008, pp. 1267-1271.

[15] J.M. Blanco, F. Peña, Obtención del valor real de las pérdidas de difícil evaluación aplicables al cálculo de rendimiento de calderas, Inf. Tecnol, 17/3, 2006, pp. 123-128.

[16] J.M. Blanco, L. Vazquez, F. Peña, Investigation on a new methodology for thermal power plant assessment through live diagnosis monitoring of selected process parameters; application to a case study, Energy, 42, 2012, pp. 170-180.

[17] J. Chacón, J.M. Sala, J.M. Blanco, Investigation on the Design and Optimization of a Low NOx-CO Emission Burner both experimentally and through CFD simulations, Energy and Fuels, 21, 2006, pp. 42-58.

[18] R.J. Kee, F.M. Rupley, J.A. Miller, M.E. Coltrin, J.F. Grcar, E. Meeks, et al, CHEMKIN v. 4.0, Technical Report San Diego, CA, Reaction Design, Inc., 2004.

[19] M. Talei, M.J. Brear, E.R. Hawkes, A comparative study of sound generation by laminar, combusting and non-combusting jet flows, Theor. *Comput. Fluid Dyn*., 2014, 28, pp. 385-408.

[20] M.S. El-Azab, K.M. Abdelgaber, Finite element solution of nonlinear diffusion problems, Applied Mathematics and Computation, 217/13, 2011, pp. 6198-6205.

[21] J. Nagler, Laminar boundary layer model for power-law fluids with non-linear Viscosity, *WSEAS Transactions on fluid mechanics*, 9, 2014, pp. 19-25.

[22] http://geolab.larc.nasa.gov/APPS/YPlus/.

[23] A. Corsini, C. Iossa, F. Rispoli, T. E. Tezduyar, A DRD finite element formulation for computing turbulent reacting flows in gas turbine combustors, *Comput Mech*, 2010, 46, pp. 159-167.

[24] F. Hamba, Analysis of filtered Navier-Stokes equation for hybrid RANS/LES simulation, Physics of Fluids, 23/1, 2011, pp.123-131.

[25] A. Alexiadis, M.P. Dudukovic, P. Ramachandran, A. Cornell, J.Wanngård, A. Bokkers, Transition to pseudo-turbulence in a narrow gas-evolving Channel, Theor. Comput. Fluid Dyn, 2012, 26, pp. 551-564.

[26] R. Siegel, J.R. Howell, *Thermal Radiation Heat Transfer*. Hemisphere Publishing Corporation, Washington D.C., 1992.

[27] G.D. Raithby, E.H. Chui., A Finite-Volume Method for Predicting a Radiant Heat Transfer in Enclosures with Participating Media. *J. Heat Transfer*, 112, 1990, p. 415-23.

[28] K.N. Bray, N. Peters, Laminar Flamelets in Turbulent Flames. In Libby, P.A. and Williams, F.A. editors, *Turbulent Reacting Flows,* Academic Press, 1994, p. 63-114.

[29] N. Peters, Turbulent combustion, Cambridge University Press, Cambridge, 2000.

[30] J. Warnatz, U. Maas, R.W. Dibble, Combustion. (3rd ed.), Springer, Heidelberg, 2001.

[31] P.J. Coelho, N. Peters. Numerical simulation of a Mild Combustion burner. Combust Flame **124,** 2001, p. 503–18.

[32] L. Kotek, V. Pistek, M. Jonak, Bivariate Process Capability Analysis of Fuel Injection Nozzles Production, *WSEAS Transactions on environment and development*, 10, 2014, pp. 491-495.

[33] Özdemir, I.B. and Peters, N. Characteristics of the reaction zone in a combustor operating at Mild Combustion. Exp Fluids **30** 6, 2001, p. 683–95.

[34] Hanson, R.K. and Salimian, S., Survey of Rate Constants in H/N/O Systems. In Gardiner, W.C., editor, *Combustion Chemistry*, 1984, p. 361.

[35] C.P. Fennimore, Formation of Nitric Oxide in Premixed Hydrocarbon Flames. In *13th Symp. (Int.) on Combustion,* The Combustion Institute, 1971, p. 373.

[36] F.J. Barnes, J.H. Bromly, T.J. Edwards, R. Madngezewsky, NOx Emissions from Radiant Gas Burners. *Journal of the Institute of Energy,* 155, 1988, p.184-88.

[37] R.W. Schefer, m. Namazian, J. Kelly, In *Combustion Research Facility News,* volume 3, number 4. Sandia, 1991.

[38] F. Backmier, K.H. Eberius, T. Just., *Comb. Sci. Tech.,* 7, 1973, p. 77.

[39] G.G. De Soete. Overall Reaction Rates of NO and N_2 Formation from Fuel Nitrogen. In *15th Symp. (Int.) on Combustion,* The Combustion Institute, 1975, p. 1093-102.

[40] J.A. Miller, C.T. Bowman, Mechanism and Modeling of Nitrogen Chemistry in Combustion. *Prog. in Energy and Comb. Sci.*, 15:287-338, 1989.

[41] J.A. Miller, G.A. Fisk, *Chemical and Engineering News*, 31, 1987.

[42] T.J. Houser, M. Hull, R. Alway, T. Biftu, *Int. Journal of Chem. Kinet.,* 12, 1980, p. 579.

[43] J.M. Blanco, L. Vazquez, F. Peña, D. Diaz, New Investigation on Diagnosing Steam Production Systems from Multivariate Time Series Applied to Thermal Power Plants, Appl. Energy, 101, 2013, pp. 589-599.

[44] S.C. Kong, R.D. Reitz, Application of detailed chemistry and CFD for predicting direct injection HCCI engine combustion and emissions, Proc. Combust. Inst., 29, 2002, pp. 663-669.

[45] F.C. Lockwood, C.A. Romo-Millanes, Mathematical Modelling of Fuel - NO Emissions From PF Burners. *J. Int. Energy,* 65, 1992, p. 144-52.

[46] C. Westbrook, F. Dryer, Simplified Reaction Mechanisms for Oxidation of Hydrocarbon Fuels in Flames. *Comb. Sci. Tech*, 27, 1981, p. 31-43.

[47] V. Zimont, Gas Premixed Combustion at High Turbulence. Turbulent Flame Closure Model Combustion Model, *Experimental Thermal and Fluid Science*, 21, 2000, p.179-86.

[48] V. Zimont, F. Biagioli, K.J. Syed, Modelling Turbulent Premixed Combustion in the Intermediate Steady Propagation Regime. *Progress in Computational Fluid Dynamics,* 1(1), 2001, p. 14-28.

[49] R.S. Barlow, G.J. Fiechtner, C.D. Carter, J.Y. Chen, Experiments on the Scalar Structure of Turbulent CO/H_2 /N_2 Jet Flames. *Combustion and Flame*, 120, 2000, p. 549-69.

[50] P. Glarborg, J.E. Johnsson, K. Dam-Johansen, Kinetics of Homogeneous Nitrous Oxide Decomposition, *Combustion and Flame*, 99, 1994, p.523-32.

[51] R.C. Steele, P.C. Malte, D.G. Nichol, J.C. Kramlich, NOx and N_2 O in Lean-Premixed Jet-Stirred Flames. *Combustion and Flame*, 100, 1995, p. 440-49.

[52] S. Senchenko, V. Bychkov and M. Liberman, Stability limits of curved stationary flames in cylindrical tubes, *Combust Sci Technol* **166** (2001), pp. 109–130.

Jesus M. Blanco, Ph D, is Assistant Professor at the University of the Basque Country, School of Engineering, Fluids Engineering Department from 1993 and tutoring assistant lecturer at the Open University since 1997. This author became industrial engineer in 1992, (School of Engineering, University of the Basque Country), Doctor in industrial engineering in 1998 (School of Engineering, University of Navarre) and MSc by Research in (School of Engineering, Cranfield University, UK). Responsible of a Doctorate course focused on computational fluid dynamics (CFD) and assistant lecturer in this later University doing several research stays. Now is supervising three PhD..

He has published more than 20 papers both in international journals and 40 in conferences in the field of thermal engineering optimization and CFD. He leaded numerous Research Projects. Current research interests are focused on industrial optimization projects, environmental protection and CFD.

Dr. Blanco is member of the Technical Association for Air Conditioning and Cooling (ASHRAE), member of the editorial board and habitual Referee of several international journals such as Applied Thermal Engineering since 2004, member of the scientific committee of the Spanish Society for Numerical Methods in Engineering. He was awarded by the Open University in Spain for research projects in the field of minimization of the environmental impact associated to industrial processes in 2005.

Lakhdar Remaki, Ph D, is a Research professor at BCAM: Basque Centre for Applied Mathematics (Bilbao), from 2012. This author became B.S.c in Mathematics in 1991 at the USTHB University, Algiers, specialization: Partial differential equations, Master in Applied Mathematics Specialization:, partial differential equations and computational methods and finally doctor in Applied Mathematics in 1997, both in Claude Bernard University, Lyon, France. Postdoctoral Fellow at the School of Engineering (E.T.S) and Polytechnic School at Montreal, Research associate at Computational Fluid Dynamics Laboratory, McGill University, Research officer at Civil and Computational Engineering Centre, School of Engineering. Swansea University, UK, Researcher at CTA: Centre of Advanced Technologies BRP (Bombardier), Sherbrooke University 2012.

He leaded numerous Research Projects and published several papers both in international journals and conferences in the field of CFD, gas particles modeling, mesh adaptation, turbomachinery, PDE's and numerical methods.

Dr. Remaki research interests are focused on Computational Fluid Dynamics, Gas-Particles modeling, Mesh Adaptation, Delaunay Mesh Generation, Turbomachinery, Partial Differential Equations (PDEs) and Numerical Analysis

Francisco Peña, Ph D, became naval engineer in 1972, (School of Naval Engineering, University of the Basque Country) and doctor in industrial engineering in 1998 (School of Engineering, University of the Basque Country). He has been working for IBERDROLA generation corporation for more than twenty years doing relevant research progress in the field of thermal design optimization, being responsible of the operational and starting procedures of a nuclear power plant from 1975 till 1980. He became senior engineer and chief inspector of Thermal Power Plants from 1998 till 2007 and assistant lecturer from 2001 at the School of Engineering, University of the Basque Country, teaching power plants in a master's degree focused on sustainability.

He is co-author of several papers in international journals and conferences in the field of thermal energy and efficiency improvement but also in the educational innovation context.

Dr. Peña worked for a Committee based on teaching innovation procedures for power plant technicians in the field of thermal efficiency from 1980 till 1987 in several thermal power plants in Spain.